International Journal of Power Electronics and Drive System (IJPEDS)
Vol. 10, No. 1, March 2019, pp. 137~150
ISSN: 2088-8694, DOI: 10.11591/ijpeds.v10.i1.pp137-150

Output feedback nonlinear control of three-phase grid-connected PV generator

A. Yahya, H. El Fadil, M. Oulcaid
Systems Engineering Laboratory (LGS), National School of Applied Sciences (ENSA), Ibn Tofail University, Morocco

Article Info

Article history:

Received May 16, 2018
Revised Aug 18, 2018
Accepted Sep 3, 2018

Keywords:

MPPT
Nonlinear control
Nonlinear observer
Output feedback control
Renewable energy
Stability analysis

ABSTRACT

This paper addresses the problem of controlling three-phase grid connected PV system involving a PV arrays, a voltage source inverter, a grid filter and an electric grid. This paper presents three main control objectives: i) ensuring the Maximum power point tracking (MPPT) in the side of PV panels, ii) guaranteeing a power factor unit in the side of the grid, iii) and ensuring the asymptotic stability of the closed loop system. Interestingly, the present study features the achievement of the above energetic goal without resorting to sensors of currents of the grid. To this end, an output-feedback control strategy combining a state observer and a nonlinear control laws is developed. The proposed output-feedback control strategy is backed by a formal analysis showing that all control objectives are actually achieved.

Corresponding Author:

Abdelhafid Yahya,
Systems Engineering Laboratory (LGS),
National School of Applied Sciences (ENSA), Ibn Tofail University,
14000 Kénitra, Morocco.
Email: yaabha2@gmail.com

1. INTRODUCTION

It was very clear from recent studies and documentation that fossil fuels would last only a few more decades. The cost of fossil fuels has become a major challenge for all of humanity. Not only the economic value but also the environmental impacts of fossil fuels have clearly pushed us towards alternatives. The biggest alternatives that can really make a difference to sustainability, such as reducing greenhouse gas emissions and the long-term economy, are renewable energy sources (RES) such as wind and solar energy [1], [2]. PV system is increasing as a renewable source due to its advantages of little maintenance, absence of moving mechanical parts, no noise and no pollutant emission [3]. Furthermore, its cost is decreasing over the next ten years, while the deployment of PV systems continues to increase rapidly. With increasing PV penetration on the grid, eventually reaching hundreds of gigawatts (GW) of interconnected capacity, a variety of methods must be considered and implemented at different scales for a reliable and cost-effective connection into power grid.

Different control strategy for three-phase grid connected of PV modules has been largely dealt with in the specialist literature in the last few years [4]-[9]. Nevertheless, good integration of medium or large PV system in the grid may therefore require additional functionality from the inverter, such as control of reactive power. Moreover, the increase in the average size of a PV system may lead to new strategies such as eliminating the DC-DC converter, which is usually placed between the PV generator and inverter, and moving the MPPT to the inverter, which leads to increased simplicity, overall efficiency and a cost reduction. These two features are present in the three-phase inverter that is presented in this paper, with the addition of a Perturb and Observe (P&O) MPPT algorithm.

The present paper is then focusing on the problem of controlling three phase grid-connected PV power generation systems. The control objectives are threefold: (i) global asymptotic stability of the whole closed-loop control system; (ii) achievement of the MPPT for the PV array; and (iii) ensuring a grid connection with unity Power Factor (PF). These objectives should be achieved in spite the climatic variables (temperature and radiation) changes. To this end, a nonlinear controller is developed using Lyapunov design technique. A theoretical analysis is developed to show that the controller actually meets its objectives a fact that is confirmed by simulation.

The paper is organized as follows: the three-phase grid connected PV system is described and modeled in Section 2. Section 3 is devoted to controller design and analysis. The controller tracking performances are illustrated by numerical simulation in Section 4.

2. RESEARCH METHOD

2.1. System overview

The main circuit of three-phase grid-connected photovoltaic system as shown in Figure 1. It consists of a PV arrays; a DC link capacitor C; a three phase inverter (including six power semiconductors) that is based upon to ensure a DC-AC power conversion and unity power factor; an inductor filter L with a series resistance r, and an electric grid. The control inputs of the system are a PWM signals u_a, $u_b$and u_c taking values in the set {0,1}. The grid voltages v_{ga}, v_{gb} and v_{gc} constitute a three-phase balanced system.

2.2. PV Array model

An equivalent circuit for a PV cell as shown in Figure 2. Its current characteristic can be found in many places [10]-[13] and presents the following expression.

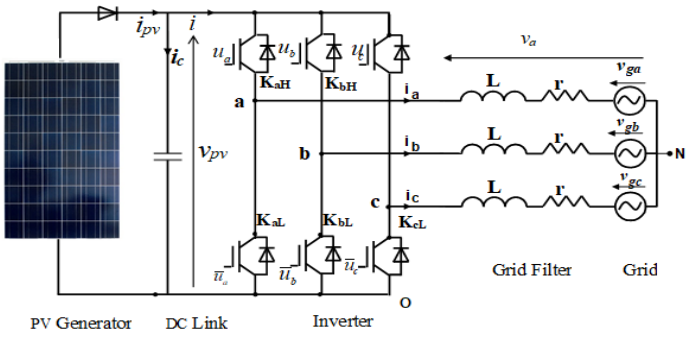

Figure 1. Three-phase grid connected PV system

$$I = I_{ph} - I_{sat}\left[\exp\left(\frac{q(V+IR_s)}{AkT}\right)-1\right]-\frac{V+IR_s}{R_{sh}} \quad (1)$$

Where

$$\begin{cases} I_{sat} = I_{satr}\left[\dfrac{T}{T_r}\right]^3 \exp\left[\dfrac{qE_{G0}}{Ak}\left(\dfrac{1}{T_r}-\dfrac{1}{T}\right)\right] \\ I_{ph} = \left[I_{phr} + K_I(T-298)\right]\lambda \end{cases} \quad (2)$$

The meaning and typical values of the parameters given by (1) and (2) can be found in many places (see e.g. [14], [15], [16]). A is diode ideal factor, k is Boltzmann constant , T is temperature on absolute scale in K, q is electron charge and λ is the radiation in kW/m^2, I_{phr} is the short-circuit current at 298 K and 1 kW/m^2, K_I = 0.0017A/K is the current temperature coefficient at I_{phr}, E_{G0} is the band gap for silicon, is reference temperature, I_{satr} is cell saturation current at T_r. PV array consists of N_s cells in series formed the panel and of N_p panels in parallel according to the rated power required. The output voltage and current can be given by the following (3) and (4).

$$v_{pv} = N_s\left(V_d - R_s I\right) \tag{3}$$

$$i_{pv} = N_p I \tag{4}$$

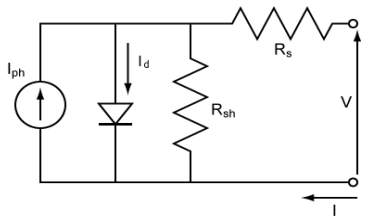

Figure 2. Solar cell circuit diagram

The photovoltaic generator considered in this paper consists of several NU-183E1 modules. The corresponding electrical characteristics of PV modules are shown in Table 1. The associated power-voltage (P-V) characteristics under changing climatic conditions (temperature and radiation) are shown in Figures 3 and 4. This highlights the Maximum Power Point (MPP) M1 to M5, whose coordinates are given in Table 3. The data in Table 1 to Table 3 will be used for simulation.

Table 2 shows the main characteristics of the PV array, designed using Sharp NU-183E1 modules connected in a proper series-parallel, making up a peak installed power of 71 kW. As there is no DC-DC converter between the PV generator and the inverter, the PV array configuration should be chosen such that the output voltage of the photovoltaic generator is adapted to the requirements of the inverter. In this case a 380V grid has been chosen, so the inverter would need at least 570V DC bus in order to be able to operate correctly. The minimum number of modules connected in series should be determined by the value of the minimum DC bus voltage and the worst-case climatic conditions. The PV array was found to require 28 series connected modules per string.

Table 1. Electrical specifications for the solar module NU-183E1

Parameter	Symbol	Value
Maximum Power	Pm	183W
Short circuit current	I_{scr}	8.48A
Open circuit voltage	V_{oc}	30.1V
Maximum power voltage	V_m	23.9V
Maximum power current	I_m	7.66A
Number of parallel modules	Np	1
Number of series modules	Ns	48

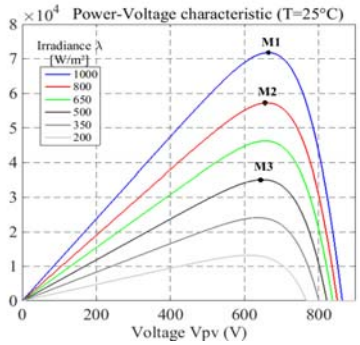

Figure 3. (P-V) characteristics of The PV Generator (NP=14 And NS=28) with constant temperature and varying radiation

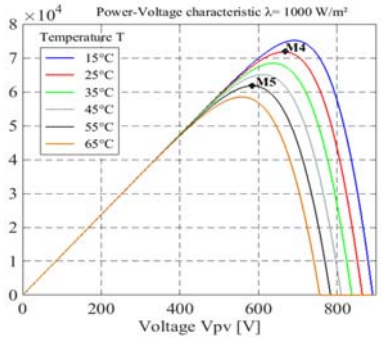

Figure 4. (P-V) characteristics of The PV Generator (NP=14 And NS=28) with constant radiation and varying temperature

Table 2 : PV Array specifications using sharp NU-183E1

Parameter	Symbol	Value
Total peak power	Ptm	71 kW
Number of series strings	NS	28
Number of parallel	NP	14
Number of PV panels	N	392
Voltage in maximum power	Vm	664V
Current peak	Im	107A

Table 3. Maximum power points (MPP): in Figure 3 and Figure 4

MPP	Vm [V]	Pm [KW]
M1	664.2	71
M2	661	57.2
M3	648.8	35.1
M4	664.2	71.5
M5	584	61.7

2.3. Modeling of three-phase grid-connected PV system

The state-space model of a three-phase grid-connected photovoltaic system shown in Figure 1 can be obtained by the dynamic equations described in (5a)-(5d):

$$\frac{d}{dt}i_a = -\frac{r}{L}i_a + \frac{v_{pv}}{3L}\left(2u_a - u_b - u_c\right) - \frac{1}{L}v_{ga} \tag{5a}$$

$$\frac{d}{dt}i_b = -\frac{r}{L}i_b + \frac{v_{pv}}{3L}\left(-u_a + 2u_b - u_c\right) - \frac{1}{L}v_{gb} \tag{5b}$$

$$\frac{d}{dt}i_c = -\frac{r}{L}i_c + \frac{v_{pv}}{3L}\left(-u_a - u_b + 2u_c\right) - \frac{1}{L}v_{gc} \tag{5c}$$

$$\frac{d}{dt}v_{pv} = \frac{1}{C}i_{pv} - \frac{1}{C}\left(u_a i_a + u_b i_b + u_c i_c\right) \tag{5d}$$

Where: $u_i = \begin{cases} 1 \rightarrow K_{iH} : on;\ K_{iL} : off \\ 0 \rightarrow K_{iH} : off;\ K_{iL} : on \end{cases}$

Applying the Concordia transformation to (5a-d), the instantaneous model in stationary coordinates is givens as (6a)-(6b):

$$\frac{d}{dt}i_\alpha = -\frac{r}{L}i_\alpha + \frac{v_{pv}}{L}u_\alpha - \frac{1}{L}v_{g\alpha} \tag{6a}$$

$$\frac{d}{dt}i_\beta = -\frac{r}{L}i_\beta + \frac{v_{pv}}{L}u_\beta - \frac{1}{L}v_{g\beta} \tag{6b}$$

$$\frac{d}{dt}v_{pv} = -\frac{1}{C}\left(u_\alpha i_\alpha + u_\beta i_\beta\right) + \frac{1}{C}i_{pv} \tag{6c}$$

where

$$\left[i_{\alpha\beta o}\right] = \left[\Theta_{abc}^{\alpha\beta o}\right]\left[i_{abc}\right];\ \left[v_{g\alpha\beta o}\right] = \left[\Theta_{abc}^{\alpha\beta o}\right]\left[v_{gabc}\right];\ \left[u_{\alpha\beta o}\right] = \left[\Theta_{abc}^{\alpha\beta o}\right]\left[u_{abc}\right] \tag{7a}$$

And the transformation matrix $\Theta_{abc}^{\alpha\beta o}$ is given by:

$$\Theta_{abc}^{\alpha\beta o} = \sqrt{\frac{2}{3}}\begin{bmatrix} 1 & -\frac{1}{2} & -\frac{1}{2} \\ 0 & \frac{\sqrt{3}}{2} & -\frac{\sqrt{3}}{2} \\ \frac{1}{\sqrt{2}} & \frac{1}{\sqrt{2}} & \frac{1}{\sqrt{2}} \end{bmatrix} \tag{7b}$$

According to the three-phase instantaneous active and reactive power theory, the instantaneous active power *P* and the instantaneous reactive power *Q* can be derived in three-phase *abc* coordinates for the three-phase photovoltaic grid-connected inverter:

$$P = v_{ga}i_a + v_{gb}i_b + v_{gc}i_c \tag{8a}$$

$$Q = \left[\left(v_{ga} - v_{gb}\right)i_c + \left(v_{gb} - v_{gc}\right)i_a + \left(v_{gc} - v_{ga}\right)i_b\right]/\sqrt{3} \tag{8b}$$

In the $\alpha\beta$ coordinates, the instantaneous active power *P* and the instantaneous reactive power *Q* can be expressed as following:

$$P = v_{g\alpha}i_\alpha + v_{g\beta}i_\beta \tag{9a}$$

$$Q = v_{g\beta}i_\alpha - v_{g\alpha}i_\beta \tag{9b}$$

3. OUTPUT FEEDBACK CONTROLLER DESIGN

The model (6a-c) is useful to build an accurate simulator for the studied system however it is not adequate to elaborate a continuous controller as it involves a binary input u_α and u_β. For control design purpose, it is more convenient to consider the following averaged model, obtained by averaging the model (6a-c) over one switching period [17].

$$\dot{x}_1 = -\frac{r}{L}x_1 + \frac{x_3}{L}\mu_\alpha - \frac{1}{L}v_{g\alpha} \tag{10a}$$

$$\dot{x}_2 = -\frac{r}{L}x_2 + \frac{x_3}{L}\mu_\beta - \frac{1}{L}v_{g\beta} \tag{10b}$$

$$\dot{x}_3 = -\frac{1}{C}\left(\mu_\alpha x_1 + \mu_\beta x_2\right) + \frac{1}{C}i_{pv} \tag{10c}$$

where x_1 , x_2 , x_3 , μ_α and μ_β denote the average values of, respectively i_α , i_β , v_{pv} , u_α and u_β . The signals μ_α and μ_β, called duty ratios which belong to $[0,1]$, are considered as the inputs of the system (10a-c).

On the basis of (10a-c), the next two subsections will be devoted to the observer design and the nonlinear controller design.

3.1. Observer design

Let us now consider in (10a-c) that is the only measurable variable. Then the following nonlinear observer is proposed:

$$\dot{\hat{x}}_1 = -\frac{r}{L}\hat{x}_1 + \frac{\hat{x}_3}{L}\mu_\alpha - \frac{1}{L}v_{g\alpha} \tag{11a}$$

$$\dot{\hat{x}}_2 = -\frac{r}{L}\hat{x}_2 + \frac{\hat{x}_3}{L}\mu_\beta - \frac{1}{L}v_{g\beta} \tag{11b}$$

$$\dot{\hat{x}}_3 = -\frac{1}{C}\left(\mu_\alpha \hat{x}_1 + \mu_\beta \hat{x}_2\right) + \frac{1}{C}i_{pv} + \lambda(x_3 - \hat{x}_3) \tag{11c}$$

Where $\hat{x}_1$, $\hat{x}_2$, $\hat{x}_3$ represent the estimates of the state variables and $\lambda > 0$ being the observer design parameter.

Let us introduce the estimation errors $z_1 = x_1 - \hat{x}_1$, $z_2 = x_2 - \hat{x}_2$ and $z_3 = x_3 - \hat{x}_3$. Then, from (10a-c) and (11a-c), one has:

$$\dot{z}_1 = -\frac{r}{L} z_1 + \frac{z_3}{L} \mu_\alpha \tag{12a}$$

$$\dot{z}_2 = -\frac{r}{L} z_2 + \frac{z_3}{L} \mu_\beta \tag{12b}$$

$$\dot{z}_3 = -\frac{1}{C}\left(\mu_\alpha z_1 + \mu_\beta z_2\right) - \lambda z_3 \tag{12c}$$

From the error system (12a-c), one can state the following:
Proposition: Consider the estimation error system (12a-c), obtained by combining the system (10a-c) and the nonlinear observer (11a-c). Then, $\exists \lambda_0$, $\forall \lambda > \lambda_0$, whatever the initial conditions, the state estimation error $z = \left[z_1, z_2, z_3\right]^T$ converges exponentially to zero.
Proof: Consider the following quadratic Lyapunov function:

$$V_o = \frac{1}{2}\sum_{i=1}^{3} z_i^2 \tag{13}$$

Its derivative, using (12a-c), can be obtained as follows:

$$\dot{V}_o = -\frac{r}{L} z_1^2 - \frac{r}{L} z_2^2 - \lambda z_3^2 + \beta_1 z_1 z_3 + \beta_2 z_2 z_3 \tag{14a}$$

With

$$\beta_1 = \mu_\alpha\left(\frac{1}{L} - \frac{1}{C}\right) \quad , \quad \beta_2 = \mu_\beta\left(\frac{1}{L} - \frac{1}{C}\right) \tag{14b}$$

Using Young's Inequality (14a) becomes

$$\dot{V}_o \le -\frac{r}{L} z_1^2 - \frac{r}{L} z_2^2 - \lambda z_3^2 + \left|\beta_1\right|\left(\frac{1}{2\varepsilon_1} z_1^2 + \frac{\varepsilon_1}{2} z_3^2\right) + \left|\beta_2\right|\left(\frac{1}{2\varepsilon_2} z_2^2 + \frac{\varepsilon_2}{2} z_3^2\right) \tag{15}$$

where ε_1 and ε_2 being any real positive constants.
As $\mu_\alpha \in [0,1]$ and $\mu_\beta \in [0,1]$ (duty ratio functions), it follows that $\left|\beta_1\right| \le \beta_0$ and $\left|\beta_2\right| \le \beta_0$ where

$$\beta_0 = \left|\frac{1}{L} - \frac{1}{C}\right| \tag{16}$$

From (15) becomes, using (16)

$$\dot{V}_o \le -k_1 z_1^2 - k_2 z_2^2 - k_3 z_3^2 \tag{17a}$$

Where

$$k_1 = \frac{r}{L} - \frac{\beta_0}{2\varepsilon_1} \quad k_2 = \frac{r}{L} - \frac{\beta_0}{2\varepsilon_2} \quad k_3 = \lambda - \frac{\beta_0}{2}\left(\varepsilon_1 + \varepsilon_2\right) \tag{17b}$$

Let ε_1 and ε_2 to be chosen as follows: $\varepsilon_1 > \frac{\beta_0 L}{2r}$ and $\varepsilon_2 > \frac{\beta_0 L}{2r}$. Then, the observer design parameter λ can be chosen so that $\lambda > \lambda_0$ where:

$$\lambda_0 = \frac{\beta_0}{2}(\varepsilon_1 + \varepsilon_2) \tag{18}$$

Therefore $k_1 > 0$, $k_2 > 0$ and $k_3 > 0$. It follows that (17a) can be rewritten as follows:

$$\dot{V}_o \leq -kV_o \tag{19}$$

where

$$k = 2\min(k_1, k_2, k_3) \tag{20}$$

From (19), it is easy to show that:

$$V_o(t) \leq -e^{-k(t-t_0)}V_o(t_0) \tag{21}$$

which yields that $V_o(t)$ is exponentially vanishing. It follows that $\lim_{t\to\infty} z(t) = 0$, which in turn shows that the estimates converge toward their true values. This ends the proof of the Proposition. In the next subsection, we focus on elaborating a controller that stabilizes the system.

3.2. Nonlinear controller design

With the aim of design an appropriate control for the model (10a-c) described in previous section, the control objectives, the control design and stability analysis will be investigated in this Section, taking into account the nonlinear feature and the multi-input multi-output (MIMO) aspect of the system. In order to define the control strategy, the first step is to establish control objectives, which can be summarized as follows:

a. Maximum power point tracking (MPPT) of PV arrays,
b. Unity power factor (PF) in the grid,
c. Asymptotic stability of the whole system.

It is worth noting that all objectives must be achieved without sensing all variables. The PV voltage x_3 is the only measurable variable.

The first control objective is to enforce the real power *P* to track the maximum power point P_M. It's already point out; that this power can be controlled by the *α-axis* current i_α and *β-axis* current i_β (see (9a)). In this paper the MPPT algorithm based on the Perturb and Observe (P&O) technique [18] is resorted to generate the coefficient θ (involved in (22)) so that the active power *P* tracks its maximum value i.e. $P = P_M$.

The second control objective means that the grid currents, i_a, i_b and i_c should be sinusoidal and in phase with the AC grid voltage v_{ga}, v_{gb} and v_{gc} respectively. To this end the reactive power have to be null. To achieve this objectives it suffices to enforce the α-axis current i_α and β-axis current i_β to track reference signals, say x_1^* and x_2^*, of the following forms:

$$x_1^* = \theta \cdot v_{g\alpha} \tag{22}$$

$$x_2^* = \theta \cdot v_{g\beta} \tag{23}$$

With θ is any real positive parameter (although transient time-variations are allowed). Its generation will be seen later using the MPPT algorithm (see section 4). Once the control objectives are clearly defined, as the MIMO system is highly nonlinear, a Lyapunov based nonlinear control is proposed [17]. Given the observer guarantees that the errors $z_1 = x_1 - \hat{x}_1$ and $z_2 = x_2 - \hat{x}_2$ converge to zero, the following controller design will be based on the estimate variables instead of their true values. Therefore, the following errors are introduced:

$$z_4 = \hat{x}_1 - x_1^* \tag{24}$$

$$z_5 = \hat{x}_2 - x_2^* \tag{25}$$

In order to achieve the objectives: MPPT and power factor unit, one can seek that the errors z_4 and z_5 are vanishing. To these ends the dynamics of z_4 and z_5 have to be clearly defined. Deriving (24) and (25), it follows from (11a) and (11b) that:

$$\dot{z}_4 = -\frac{r}{L}\hat{x}_1 + \frac{\hat{x}_3}{L}\mu_\alpha - \frac{1}{L}v_{g\alpha} - \dot{x}_1^* \tag{26}$$

$$\dot{z}_5 = -\frac{r}{L}\hat{x}_2 + \frac{\hat{x}_3}{L}\mu_\beta - \frac{1}{L}v_{g\beta} - \dot{x}_2^* \tag{27}$$

The goal, now, is to make z_4 and z_5 exponentially vanishing by enforcing its derivatives $\dot{z}_4$ and $\dot{z}_5$ to behave as follows:

$$\dot{z}_4 = -\rho_1 \operatorname{sgn}(z_4) - \xi_1 \int z_4(\tau) d\tau \tag{28}$$

$$\dot{z}_5 = -\rho_2 \operatorname{sgn}(z_5) - \xi_2 \int z_5(\tau) d\tau \tag{29}$$

where $\rho_1 > 0$, $\rho_2 > 0$, $\xi_1 > 0$ and $\xi_2 > 0$ being design parameters and is a signum function. It is worth noting that the integral actions are introduced in (28) and (29) to allow a good robustness of the controller against unmodeled dynamics and perturbations. Combining (26) and (28) the first control law μ_α is obtained:

$$\mu_\alpha = \frac{L}{\hat{x}_3}\left(-\rho_1 \operatorname{sgn}(z_4) + \frac{r}{L}\hat{x}_1 + \frac{1}{L}v_{g\alpha} + \dot{x}_1^* - \xi_1 \int z_4(\tau) d\tau\right) \tag{30}$$

Finally, combining (27) and (29), the second control law μ_β is also obtained

$$\mu_\beta = \frac{L}{\hat{x}_3}\left(-\rho_2 \operatorname{sgn}(z_5) + \frac{r}{L}\hat{x}_2 + \frac{1}{L}v_{g\beta} + \dot{x}_2^* - \xi_2 \int z_5(\tau) d\tau\right) \tag{31}$$

Since the control laws are clearly defined, the concern now is to investigate the convergence of the errors z_4 and z_5. To this end the following quadratic Lyapunov function is considered

$$V_C = \frac{1}{2}{z_4}^2 + \frac{1}{2}{z_5}^2 + \frac{\xi_1}{2}\left[\int z_4(\tau) d\tau\right]^2 + \frac{\xi_2}{2}\left[\int z_5(\tau) d\tau\right]^2 \tag{32}$$

Its derivative is obtained as follows Its derivative is obtained as follows:

$$\dot{V}_C = z_4 \dot{z}_4 + z_5 \dot{z}_5 + \xi_1 z_4 \left[\int z_4(\tau) d\tau\right] + \xi_2 z_5 \left[\int z_5(\tau) d\tau\right] \tag{33}$$

which, using (28) and (29), gives:

$$\dot{V}_C = -\rho_1 |z_4| - \rho_2 |z_5| \tag{34}$$

As V_c is positive definite function and its derivative (34) is negative definite it follows that the equilibrium $(z_4, z_5) = (0,0)$ is globally asymptotically stable [18]. Which, in turn, gives $\lim_{t\to\infty}(z_4(t), z_5(t)) \to (0,0)$

The main result of the proposed output feedback controller is summarized in the following theorem.

Theorem: Consider the closed-loop system consisting of the controlled system of Figure 1 represented by its nonlinear model (10a-c), the nonlinear observer (11a-c) and the controller composed of the control laws (30) and (31). Then, one has:

a. The closed loop system is GAS. It follows that all closed loop signals are bounded.

b. The estimation errors $z=[z_1,z_2,z_3]^T$ converges exponentially to zero.

c. The tracking errors z_4 and z_5 converge to zero implying MPPT achievement and power factor unit.

Proof: let us consider the following quadratic Lyapunov function:

$$V=V_O+V_C=\frac{1}{2}\sum_{i=1}^{5}z_i^2+\frac{\xi_1}{2}\left[\int z_4(\tau)d\tau\right]^2+\frac{\xi_2}{2}\left[\int z_5(\tau)d\tau\right]^2 \quad (35)$$

Its derivate, using (19) and (34), can be obtained as follows:

$$\dot{V}=\dot{V}_O+\dot{V}_C\le-\frac{k}{2}\left(z_1^2+z_2^2+z_3^2\right)-\rho_1|z_4|-\rho_2|z_5| \quad (36)$$

Which clearly shows that, the equilibrium $z=0$ of the closed loop system with the state error vector $z=[z_1,z_2,z_3,z_4,z_5]^T$ is globally asymptotically stable. It follows that all errors are vanishing. This ends the proof of theorem. The next section devoted to the performances evaluation of the proposed output feedback controller.

4. SIMULATION RESULTS

The theoretical performances described by the theorem of an output feedback controller, including the control laws (30-31) and the nonlinear observer (11a-c), designed in Section 3, are now illustrated by simulation. The experimental setup, described by Figure 5, is simulated using MATLAB/SIMULINK. The characteristics of the controlled system are listed in Table 4. Note that the controlled system is simulated using.

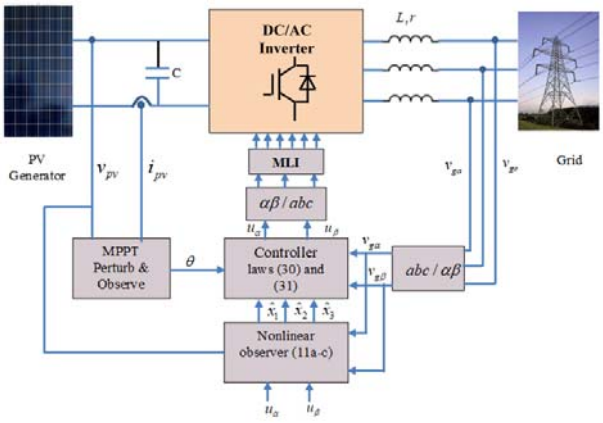

Figure 5. Simulation bench of the proposed three-phase grid connected system

The instantaneous three phase model given by (5a-d).The model (10a-c) in α-β axis is only used in the controller design. The design parameters of the controller are given values of Table 5. These parameters have been selected using a 'trial-and-error' search method and proved to be suitable. It worth noting that the parameter θ involved in (22) and (23) is generated using Perturb and Observe algorithm with the block-diagram illustrated by Figure 6. The resulting closed loop control performances are illustrated by Figure 7 to Figure 13.

Table 4. Characteristics of controlled system

Parameter	Symbol	Value
PV array	PV power	40 kW
DC link capacitor	C	3300μF
Grid filter inductor	L	3mH
	r	0.2Ω
PWM	Switching frequency	10kHz
Grid	AC source	220V
	Line frequency	50Hz

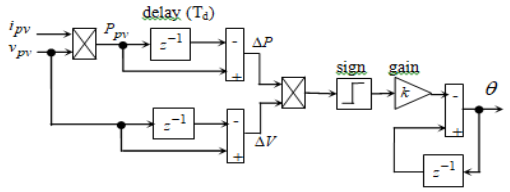

Figure 6. P&O algorithm implementation in Matlab/Simulink software

Table 5. Controller parameters

Parameter	Symbol	Value
Design parameters	ρ_1	10^3
	ρ_2	4×10^3
	ξ_1	0.1
	ξ_2	0.1
	λ	5×10^5
P&O algorithm parameters	*Delay time* T_d	10^{-4}
	Step value k	0.3

4.1. Radiation change effect

Figure 7 shows the perfect MPPT in the presence of radiation step changes meanwhile, the temperature is kept constant, equal to 298.15K(25°C). The simulated radiation profile is as follow: a first step change is performed between 500 and 1000W/m² at time t = 0.1 s and the second one between 1000 and 800 W/m² at time t = 0.2 s. The Figure 8 shows that the PV power captured varies between 35.1 kW and 71 kW and then returns to 57.2 kW.These values correspond is shows in Figure 3 to maximum points (M3, M1 and M2) of the curves associated to the considered radiation, respectively. The Figure 8 also shows that the voltage of the PV array Vpv varies between V_{pv} = 648.8 V and V_{pv} = 664 V and then returns to 661V, which correspond very well to the optimum voltages. Figure 9. shows the injected current i_a and the grid voltage v_{ga} This Figure 9 clearly shows that the grid current i_a is sinusoidal and in phase with the grid voltage v_{ga}, proving that the power factor unit is achieved. The alternating currents injected to the grid are illustrated by Figure 10.

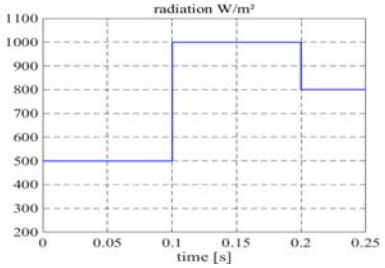

(a)

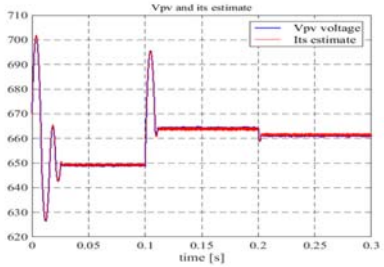

(b)

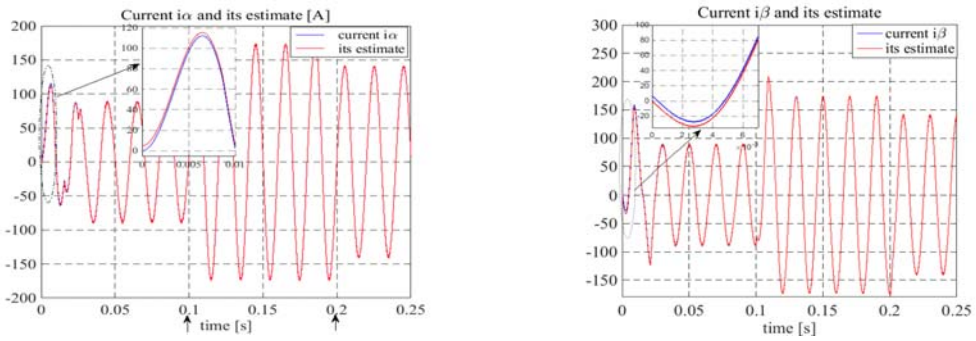

(c) (d)

Figure 7. State variables and their estimates in transitional regime and in presence of radiation step changes

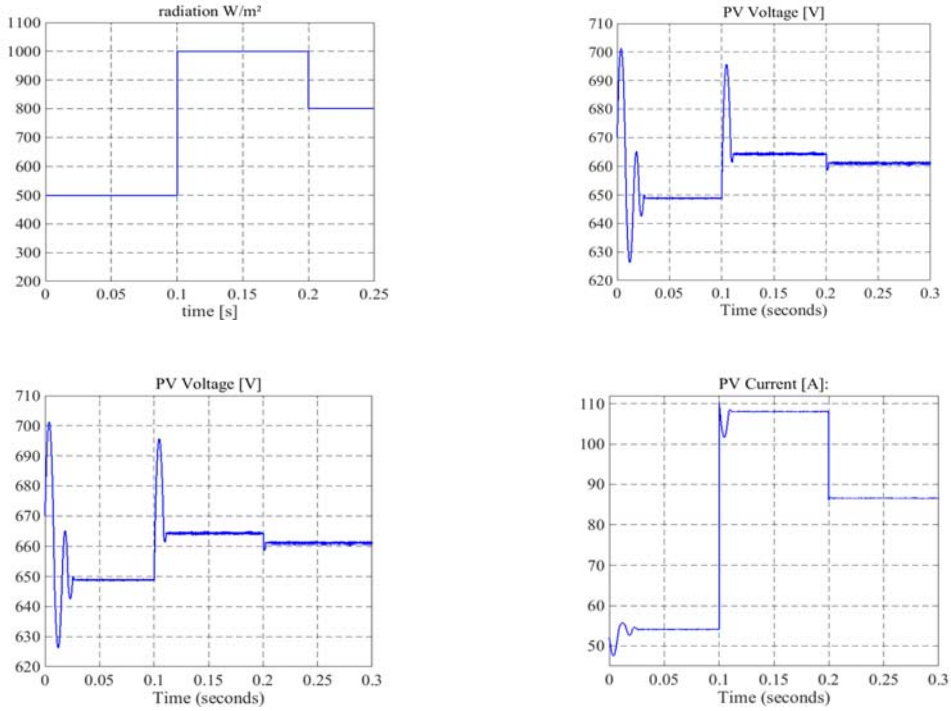

Figure 8. MPPT capability of the controller in presence of radiation step changes

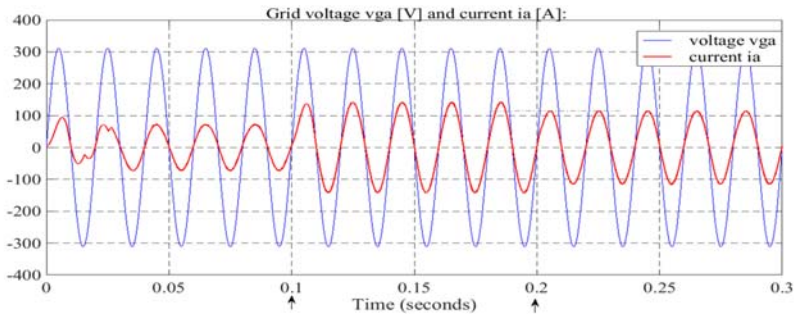

Figure 9. Unity PF achievement in presence of radiation step changes

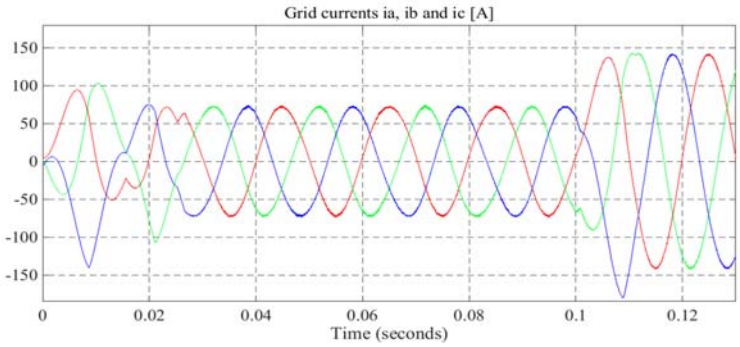

Figure 10. A zoomed waveforms of the alternating currents injected to the grid in presence of radiation step changes

4.2. Temperature variation effect

Figure 11 shows the performances of the controller in presence of temperature step changes while the radiation λ is kept constant equal to 1000W/m^2. The temperature step change is performed at time t=0.15s between T=25°C (298.15K) and T=55°C (328.15K). It is worth noting that these changes are very abrupt which is not realistic in practical case. Nevertheless, with this important change we want to show a good robustness of the proposed controller to achieving the MPPT objective. It can be seen from Figure 11 that the system tracks the new operating point very quickly. Indeed, the captured PV power P achieves the values 71.7kW et 61.7kW corresponding to the maximum points (M4 and M5) associated to the temperatures 25°C and 55°C, respectively as shown in Figure 4.

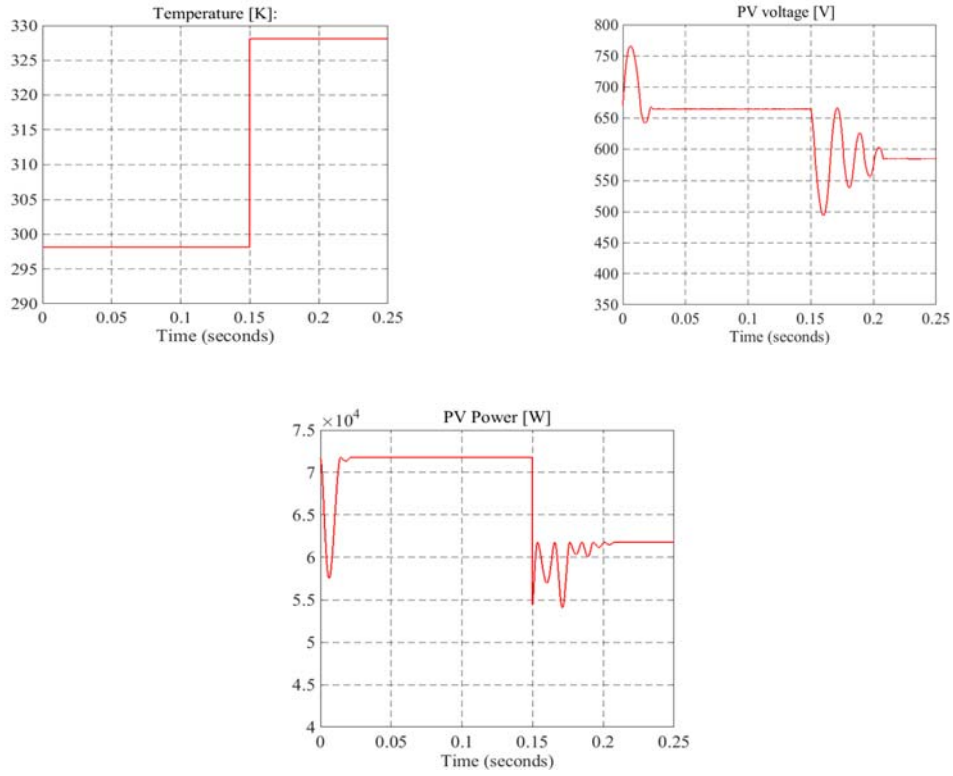

Figure 11. MPPT and DC bus voltage behavior in presence of temperature step changes

Figure 12 illustrates the grid current i_a and the grid voltage v_{ga}, Figure 12 also shows that the current i_a is sinusoidal and in phase with the voltage v_{ga} which proves the unity PF requirement. Finally, Figure 13 shows the zoomed three phase's grid currents and voltages.

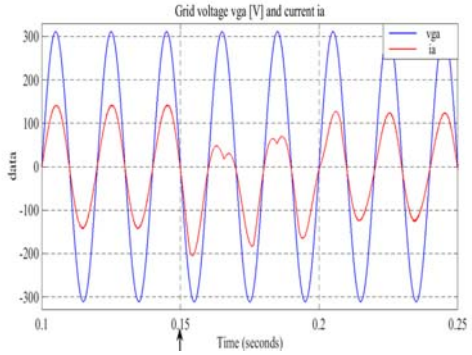

Figure 12. Unity PF behavior in presence of temperature changes

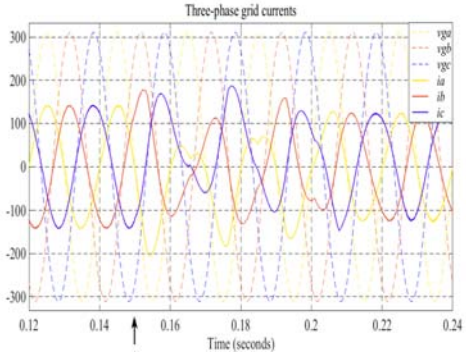

Figure 13. Zoomed grid currents and voltages in presence of temperature step changes

5. CONCLUSION

We have addressed the problem of current sensorless control of the photovoltaic energy conversion system. The main feature of the system presented is it does not require an intermediate stage of DC-DC control, because the maximum power is set by the inverter itself by means of a Perturb & Observe algorithm.

The system dynamics has been described by the nonlinear state-space model (5a-b). Based on a transformed model in $\alpha - \beta$ axis, an output feedback controller, combining an observer and a state feedback control laws is designed and analyzed using a Lyapunov approach. The controller objectives are threefold: i) ensuring the MPPT in the side of PV generator; ii) guaranteeing a power factor unit in the side of the grid, iii) ensuring the global asymptotic stability of the closed loop system. Using both formal analysis and simulation, it has been proven that the obtained controller meets all the objectives. It is worth noting that all objectives are achieved without resorting to the measurement of all variables. The use of the estimator is motivated by the global cost and reliability considerations. Indeed, the fewer the number of sensors, the lower the global cost.

REFERENCES

[1] Arash Anzalchi, Arif Sarwat, "Overview of technical specifications for grid-connected photovoltaic systems, " *Energy Conversion and Management*, vol. 152, pp. 312-327, 2017.
[2] Ouya Ifaei, Abdolreza Karbassi, Gabriel Jacome, ChangKyoo Yoo, "A systematic approach of bottom-up assessment methodology for an optimal design of hybrid solar/wind energy resources – Case study at middle east region", *Energy Conversion and Management*, vol. 145, pp. 138-157, 2017.
[3] Issam Abadlia, Mohamed Adjabi, Hamza Bouzeria, "Sliding mode based power control of grid-connected photovoltaic-hydrogen hybrid system," *International Journal of Hydrogen Energy*, vol. 42, pp. 28171-28182, 2017.
[4] Schonardie, Mateus F. Martins, Denizar C., "Three-phase grid-connected photovoltaic system with active and reactive power control using dq0 transformation, "*IEEE 39th Annual Power Electronics Specialists Conference*, pp. 1202-1207, 2008.
[5] Hui Zhang, Hongwei Zhou, Jing Ren, Weizeng Liu, Shaohua Ruan and Yongjun Gao, "Three-phase grid-connected photovoltaic system with SVPWM current controller," *2009 IEEE 6th International Power Electronics and Motion Control Conference*, Wuhan, pp. 2161-2164, 2009.
[6] S. Yang, Q. Lei, F. Z. Peng and Z. Qian, "A Robust Control Scheme for Grid-Connected Voltage-Source Inverters," in *IEEE Transactions on Industrial Electronics*, vol. 58, pp. 202-212, Jan. 2011.
[7] S. Balathandayuthapani, C. S. Edrington, S. D. Henry and J. Cao, "Analysis and Control of a Photovoltaic System: Application to a High-Penetration Case Study," in *IEEE Systems Journal*, vol. 6, pp. 213-219, June 2012.
[8] M. Castilla, J. Miret, A. Camacho, J. Matas and L. G. de Vicuna, "Reduction of Current Harmonic Distortion in Three-Phase Grid-Connected Photovoltaic Inverters via Resonant Current Control," in *IEEE Transactions on Industrial Electronics*, vol. 60, pp. 1464-1472, April 2013.
[9] M. A. Mahmud, H. R. Pota, M. J. Hossain and N. K. Roy, "Robust Partial Feedback Linearizing Stabilization Scheme for Three-Phase Grid-Connected Photovoltaic Systems," in *IEEE Journal of Photovoltaics*, vol. 4, pp. 423-431, Jan. 2014.

[10] A. Yahya, H. E. Fadil, J. M. Guerrero, F. Giri and H. Erguig, "Three-phase grid-connected of photovoltaic generator using nonlinear control," *2014 IEEE Conference on Control Applications (CCA)*, Juan Les Antibes, pp. 879-884, 2014.
[11] Yaichi, Mohammed & Fellah, Mohammed-Karim & Mammeri, Abdelkrim. "A Neural Network Based MPPT Technique Controller for Photovoltaic Pumping System." *International Journal of Power Electronics and Drive System (IJPEDS)*, vol. 4, pp. 241-255, 2014.
[12] El Azzaoui, Marouane & Mahmoudi, Hassane & Boudaraia, Karima. (2016). Backstepping Control of wind and photovoltaic hybrid Renewable Energy System. *International Journal of Power Electronics and Drive Systems (IJPEDS)*. Vol. 7, pp. 677-686, 2016.
[13] A. Lekbir, C. K. Gan, M. R. A. Ghani et T. Sutikno, "The Recovery of Energy from a Hybrid System to Improve the Performance of a Photovoltaic Cell," *International Journal of Power Electronics and Drive System (IJPEDS)*, vol. 9, , pp. 957-964, September 2018.
[14] Chen-Chi Chu, Chieh-Li Chen. "Robust maximum power point tracking method for photovoltaic cells: A sliding mode control approach". *Solar Energy*, vol. 83, pp. 1370–1378, 2009.
[15] Enrique J.M., E. Duran, M. Sidrach-de-Cardona, J.M. Andujar. "Theoretical assessment of the maximum power point tracking efficiency of photovoltaic facilities with different converter topologies". *Solar Energy*, vol. 81, pp. 31-38, 2007.
[16] El Fadil, H. and Giri, F. "Climatic sensorless maximum power point tracking in PV generation systems". *Control Engineering Practice*, vol. 19, pp. 513–521, May 2011.
[17] Krein P.T., Bentsman J., Bass R. M. and Lesieutre B. "On the use of averaging for analysis of power electronic system" *IEEE Transactions on Power Electronics*, vol. 5, pp. 182–190, 1990.
[18] Khalil H. Nonlinear systems. NJ, USA: Prentice Hall; 2003.
[19] D. Sera, L. Mathe, T. Kerekes, S. V. Spataru and R. Teodorescu, "On the Perturb-and-Observe and Incremental Conductance MPPT Methods for PV Systems," in *IEEE Journal of Photovoltaics*, vol. 3, pp. 1070-1078, July 2013.

BIOGRAPHIES OF AUTHORS

Abdelhafid Yahya obtained his B.S. degree in Electrotechnical, Agrégation degree in Electrical Engineering, and M.S. degree in Electronics and Telecommunication from the University AbdelmalekSaadi of Tetouan Morocco in 1997, 2010, and 2012 respectively. Currently he is pursuing a Ph.D. in distributed energy resources at the University of IbnTofail, Kénitra, Morocco. His research interests include new energy technologies, simulation methods, power systems dynamics and control, power electronics modeling and design and renewable energy resources

Hassan El Fadil received his B.S. degree in Electronics, Agrégation degree in Electrical Mohammadia School of Engineers, Mohammed V University, Rabat, Morocco, in 1994, 1999, 2003, and 2008 respectively. Since 2011, he has been, successively Assistant Professor and Habilitated Professor in the National School of Applied Sciences, Ibn Tofail University, Kénitra, Morocco. He is currently with the LGS Laboratory, and his research interests include nonlinear and adaptive control, power converters and electric motor control, renewable energy, distributed energy resources, smart grid, and electric vehicles. He has published over 70 journal/conference papers.

Mustapha Oulcaid received his degree in Electrical Engineering (Electronic and Embedded Systems) from ENSA, Ibn Tofail University, Kenitra, Morocco, in 2014. He is currently pursuing a Ph.D. in renewable energy engineering at the same University. Since 2016, he has been an Assistant Professor with the Electrical Engineering Department at National School of Applied Sciences, Kenitra. His research interests include renewable energy, microgrids, and smartgrids.